Acoustic tuning of shear thickening suspensions: A universal scaling analysis

Anna R. Barth,[1, a)] Navneet Singh,[1] Stephen J. Thornton,[1] Pranav Kakhandiki,[1] Edward Y.X. Ong,[1] Meera Ramaswamy,[2] Abhishek M. Shetty,[3] Bulbul Chakraborty,[4] James P. Sethna,[1] and Itai Cohen[1]
[1)]*Department of Physics, Cornell University, Ithaca, New York 14850, USA*
[2)]*Department of Mechanical Engineering, University of Minnesota, Minneapolis, Minnesota 55455, USA*
[3)]*Department of Rheology, Anton Paar, Ashland, Virginia 23005, USA*
[4)]*Department of Physics, Brandeis University, Waltham, Massachusetts 02453, USA*

(Dated: 29 January 2026)

Tuning shear thickening behavior is a longstanding problem in the field of dense suspensions. Acoustic perturbations offer a convenient way to control shear thickening in real time, opening the door to a new class of smart materials. However, complete control over shear thickening requires a quantitative description for how suspension viscosity varies under acoustic perturbation. Here, we achieve this goal by experimentally probing suspensions with acoustic perturbations and incorporating their effect on the suspension viscosity into a universal scaling framework where the viscosity is described by a scaling function, which captures a crossover from the frictionless jamming critical point to a frictional shear jamming critical point. Our analysis reveals that the effect of acoustic perturbations may be explained by the introduction of an effective interparticle repulsion whose magnitude is roughly equal to the acoustic energy density. Furthermore, we show how this scaling framework may be leveraged to produce explicit predictions for the viscosity of a dense suspension under acoustic perturbation. Our results demonstrate the utility of the scaling framework for experimentally manipulating shear thickening systems.

I. INTRODUCTION

Many dense colloidal and granular suspensions shear thicken, exhibiting a viscosity which increases with shear stress, sometimes quite dramatically[1–3]. The thickening occurs when interparticle contacts transition from lubricated interactions to frictional interactions[4–8]. Such suspensions have found a variety of applications from industrial polishing to protective fabrics to impact-resistant batteries[9–11]. However, shear thickening is also responsible for a litany of engineering challenges. Shear thickening increases the power required to mix and transport dense suspensions, and in the most severe cases, can even lead to equipment damage[2,12]. Therefore there is an interest in reducing, tuning, and controlling shear thickening behavior. Many mechanisms exist to reduce shear thickening by modifying the materials that compose the suspension, for example by reducing the volume fraction of solid particles or modifying surface properties of the particles[13–18]. However, for many practical applications, the material cannot be modified. In such circumstances, it is desirable to tune the viscosity with an external control knob.

One way to control shear thickening behavior is by applying acoustic perturbations. Ultrasound acoustic perturbations have been shown to dethicken and even unjam shear thickening suspensions[19,20]. Upon application of the acoustic field, the suspension transitions to a lower-viscosity state, and the viscosity recovers once the field is removed. This rapid, reversible response allows for tuning of the suspension's viscosity in real time. Additionally, unlike other techniques for tuning suspension rheology in real time, such as magnetorheology[21] and orthogonal shear perturbations[22,23], acoustic perturbations can be easily implemented in various flow geometries simply by installing a piezoelectric transducer. These advantages make acoustic perturbations a promising tool for a wide variety of applications involving dense suspensions. However, acoustic perturbations remain poorly understood. There is currently no quantitative description for the magnitude of acoustic dethickening, and the physical cause of the effect remains elusive.

Although the effect of ultrasound on suspension rheology has not been widely studied, a somewhat larger body of work focuses on the effects of low-frequency vibrations in the range of 10-100 Hz. Low-frequency vibrations have been shown to fluidize jammed granular suspensions[24–28] and dry granular media[29,30]. In these experiments, the vibrations are described by the density of kinetic energy injected into the system. Vibrations induce Brownian-like thermal motion of the granular particles[29,31], and it has been proposed that this results in unjamming by increasing the rate at which particles escape the force-bearing network of interparticle contacts[26,27,30,32]. Recent work has also proposed that this diffusive motion can be incorporated into rheological modeling as an effective interparticle repulsion[28]. It is unclear how much of this past work will apply to ultrasound fields, where distinct physical effects such as cavitation, radiation forces, and acoustic streaming may occur[33–35]. Furthermore, the literature on low-frequency vibrations has focused on jammed suspensions rather than shear thickening suspensions.

To model the viscosity of a shear thickening suspension in an external field, a recently-developed universal scaling framework has emerged as a useful tool. In this framework, shear thickening is controlled by two jamming critical points: one frictionless and one frictional. From this perspective, the viscosity of a shear thickening suspension can be described

[a)]Author to whom correspondence should be addressed; electronic mail: ab2444@cornell.edu

by a crossover scaling function whose argument is a scaling variable that takes into account the combined contributions of shear stress and volume fraction. It has been shown that suspensions of cornstarch in glycerol and suspensions of silica microspheres in glycerol are described by the same scaling function. This universality is precisely what would be expected for a traditional universal scaling function of the variety typically derived near critical points in equilibrium statistical mechanics, leading to the hypothesis that this scaling function is indeed universal across a wide class of shear thickening suspensions[36,37].

Recently, this framework has been extended to incorporate the effects of orthogonal shear perturbations. Orthogonal shear is a common rheometric technique in which a small amplitude oscillatory shear is imposed perpendicular to the primary shear direction[38–41]. It has been applied to polymer solutions[38,42], colloidal gels[43,44], glasses[45], and solutions of micelles[46,47]. In shear thickening suspensions, orthogonal shear perturbations cause dethickening by disrupting the formation of force chains[22]. This effect can be incorporated into the universal scaling framework by a simple modification to the argument of the scaling function[23]. Remarkably, this approach offers a complete quantitative description of shear thickening suspension rheology under orthogonal shear perturbations, so that with only a few measurements in any particular system, one could map out the entire parameter space. Inspired by this past work, we seek to incorporate the effect of acoustic perturbations into the same universal scaling function.

II. METHODS

Suspensions were prepared from polydisperse aluminosilicate ceramic microspheres with a size range of $1-12\,\mu m$ (Nationwide Protective Coating, Inc.) mixed with glycerol (Ricca Chemical). Quantities of dry particles and glycerol were measured by mass in order to estimate the volume fraction of each sample, taking the density of glycerol to be $\rho_s = 1.26\,\mathrm{g/mL}$ and the density of particles to be $\rho_p = 2.4\,\mathrm{g/mL}$. Despite the density mismatch between solvent and particles, sedimentation was not a significant issue under the conditions used for measurements (see Supplementary Material for data pertaining to the system's stability). Suspensions were mixed by hand, vortexed, and sonicated for 30 minutes immediately before beginning each experiment.

Measurements were performed on an Anton Paar MCR 702 rheometer with a cone and plate geometry (diameter 50 mm, cone angle 2°, cone truncation length $211\,\mu\mathrm{m}$). In order to prevent the glycerol from absorbing water from the air, the sample was surrounded by calcium sulfate desiccant (Drierite) and kept under a plastic enclosure (Fig 1a). Under these conditions, the viscosity of the suspension was stable in time, varying by less than 15% over the time scale of the experiment (Fig. S2 in the Supplementary Material). Stress sweeps for each sample demonstrate clear shear thickening behavior (Fig. 1b).

Acoustic perturbations were applied using a custom bottom plate geometry (diameter 19 mm) with a piezoelectric disk (APC International, material 841) driven with an AC voltage at its thickness mode resonant frequency $f = 1.15\,\mathrm{MHz}$ (wavelength 1.71 mm in glycerol[48]) to supply acoustic perturbations, as previously described in past work[19,20]. The amplitude of the perturbation was controlled by the magnitude of the AC voltage driving the piezo. We quantify the strength of these perturbations by the acoustic energy density U_a[26,28], calculated as

$$U_a = \frac{1}{2}\rho_0 \delta_a^2 (2\pi f)^2 \tag{1}$$

where ρ_0 is the density of the medium, and δ_a and f are the amplitude and frequency of the acoustic oscillations. U_a is simply the density of kinetic energy transmitted by the acoustic field. We take the density of the medium to be the average density of the solvent and the solid particles $\rho_0 = \frac{1}{2}(\rho_s + \rho_p)$. We estimate the amplitude of the acoustic oscillations $\delta_a = V d_{33}$, where V is the amplitude of the AC voltage attached to the piezo and d_{33} is the piezoelectric modulus. For our experiments, V ranged from 0 V to 80 V and $d_{33} = 3\times10^{-10}\,\mathrm{m/V}$, resulting in acoustic oscillation amplitudes $\delta_a \leq 24\,\mathrm{nm}$. Potential effects arising from the strain and strain rate induced by the oscillatory motion of the bottom plate are considered in the Supplementary Material.

During experiments, a constant shear stress σ was applied via the rheometer, and then acoustic perturbations were applied for 5.0 ± 0.5 seconds each (the acoustic field was turned on and off by hand, resulting in some variation in the application time). A few representative examples of responses to acoustic perturbations are shown in Fig. 1c. At the onset of the acoustic perturbation, the suspension viscosity sharply decreased in under 0.1 seconds (the rheometer sampling time). Following this rapid drop, the viscosity exhibited a short transient increase before reaching a steady state. The application period of 5 seconds was chosen to ensure effects from these transients were minimized.[49] When the perturbation was removed, the viscosity showed a rapid increase and a more gradual return to its original value. The system was monitored manually to ensure the waiting time between measurements was sufficient for this recovery. To quantify the effect of these acoustic perturbations, we report the average viscosity for the period where the perturbations were applied. The viscosity's dependence on acoustic energy density and applied shear stress for one volume fraction ($\phi = 0.52$) is shown in Fig. 1d.

III. RESULTS

We begin by examining the viscosity η of the suspensions in the absence of an acoustic field (i.e., the data shown in Fig. 1b). Past work[23,36] recognized that the viscosity of a shear thickening suspension can be related to its volume fraction ϕ and applied shear stress σ through a Widom-like scaling function[50], inspired by the Wyart-Cates model[6]:

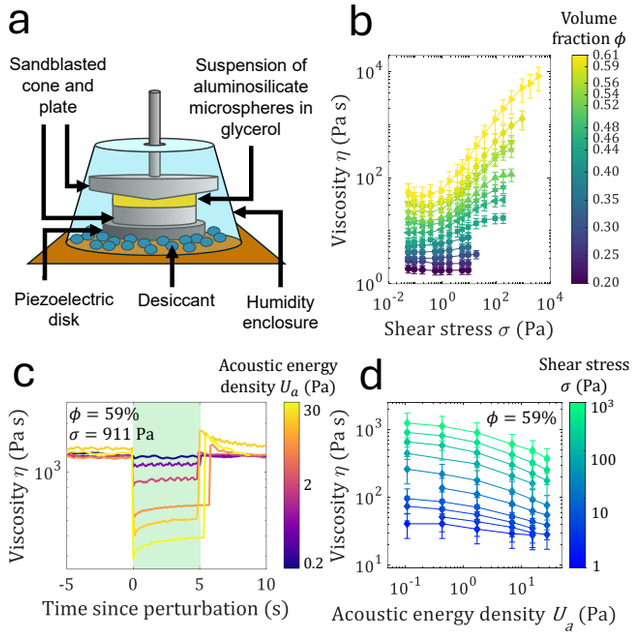

FIG. 1. Suspensions dethicken under acoustic perturbations. (a) Schematic of apparatus used to apply acoustic perturbations on the rheometer. (b) Viscosity η versus shear stress σ for various volume fractions ϕ of aluminosilicate microspheres in glycerol. (c) Viscosity versus time for a few example acoustic perturbations, applied on a suspension with volume fraction $\phi = 0.61$ and under applied shear stress $\sigma = 911\,\mathrm{Pa}$. The color shows the acoustic energy density U_a of each perturbation. (d) Viscosity versus acoustic energy density U_a for a volume fraction of $\phi = 0.52$. The applied shear stress σ is shown by the color.

$$\eta(\phi,\sigma) = (\phi_0-\phi)^{-2}\mathscr{F}\left(\frac{C(\phi)e^{-\sigma_0^*/\sigma}}{\phi_0-\phi}\right). \qquad (2)$$

Here, $\mathscr{F}$ is a crossover scaling function that captures the transition from frictionless jamming to frictional jamming. ϕ_0 is the frictionless jamming volume fraction, a material-dependent parameter related to the shape and size distribution of the particles. As in the Wyart-Cates model, σ_0^* is the shear stress required to overcome interparticle repulsion and form frictional contacts, and $f(\sigma) = e^{-\sigma_0^*/\sigma}$ represents the fraction of interparticle contacts that are frictional rather than lubricated[6]. $C(\phi)$ is the anisotropy factor, a function of volume fraction hypothesized to quantify the fraction of interparticle contacts which lie along the compressive axis and contribute to shear thickening[36]. Equation 2 identifies two renormalization group flow directions originating at the frictionless jamming point. One of these directions, $\phi_0-\phi$, simply corresponds to the distance in volume fraction to the frictionless jamming point. The other, $C(\phi)e^{-\sigma_0^*/\sigma}$, corresponds to the contribution of friction to the viscosity.[51]

Equation 2 implies that when $\eta(\phi_0-\phi)^2$ is plotted against $x = C(\phi)e^{-\sigma_0^*/\sigma}/(\phi_0-\phi)$, all data across different volume fractions and shear stresses should collapse onto a single curve $\mathscr{F}(x)$[23,36]. We seek such a collapse of the acoustics-free data by varying the parameters involved in x ($C(\phi)$, σ_0^*, and ϕ_0) according to a fitting procedure which allows all these parameters to vary simultaneously. We further assess the sensitivity of the data collapse by calculating confidence intervals for these parameters. A description of the fitting procedure, as well as a table of fit values with confidence intervals, can be found in the Supplementary Material. The resulting data collapse along with the best fit $\mathscr{F}(x)$ curve are shown in Fig. 2a and Fig. 2b.

Analysis of the scaling function $\mathscr{F}(x)$ shows it is flat for low values of x, corresponding to the low-stress regime where the viscosity controlled by the frictionless jamming point[6,36], following $\eta \sim (\phi_0-\phi)^{-2}$. Near x_c, corresponding to the high-stress regime where the viscosity is controlled by the frictional jamming point, $\mathscr{F}(x)$ diverges as a power law, $\mathscr{F}(x) \sim (x_c-x)^{-\delta}$ as shown in Fig. 2b. Note that because x contains a multiplicative factor $C(\phi)$, there is an overall scale that may be chosen for x; we choose this scale so that $x_c = 1$. We find the value of the exponent δ by fitting a functional form to $\mathscr{F}(x)$ (see Equations S8 and S9 in Supplementary Material) and find $\delta = 0.9 \pm 0.3$. Thus, as x approaches a critical value $x_c = 1$, the viscosity is controlled by the frictional jamming point[36,52] and follows $\eta \sim (\phi_J-\phi)^{-0.9}$.

The anisotropy factor $C(\phi)$ is shown in Fig 2c. $C(\phi)$ is non-monotonic in volume fraction. Previous work[23,36,53] has observed the same non-monotonicity, and attributed it to the distribution of interparticle contacts: at low volume fractions, few interparticle contacts form, while at high volume fractions, interparticle contacts form in all directions; at intermediate volume fractions, force chains proliferate along the maximum compressive axis. We note that, for low volume fractions, the confidence interval on $C(\phi)$ is rather large. This reflects the fact that low volume fractions correspond to small values of x. Since $\mathscr{F}(x)$ is nearly flat in this region, relatively large changes in x correspond to very little change in $\mathscr{F}(x)$. Therefore for lower volume fractions, there is a wide range of $C(\phi)$ over which the quality of the data collapse is still quite good.

Having analyzed the data with no acoustic perturbations (i.e. acoustic energy density $U_a = 0$), we now seek a strategy to incorporate the effect of acoustic perturbations into this framework. When data with acoustic perturbations (i.e. nonzero U_a) are plotted as $\eta(\phi_0-\phi)^2$ versus x, because of the acoustic dethickening effect, the data no longer collapse, as shown in Fig. 3a. We hypothesize that the acoustic perturbations induce some additional interparticle repulsive stress σ_a^*, which could be supplied, for example, by microstreaming effects[54,55] or by a thermal-like interaction arising from diffusive particle motion [28,56]. We also conjecture that the acoustic repulsion adds onto the pre-existing interparticle repulsion, so that the total repulsive barrier $\sigma_{\mathrm{total}}^*$ is:

$$\sigma_{\mathrm{total}}^* = \sigma_0^* + \sigma_a^*(U_a). \qquad (3)$$

Accordingly, Equation 2 becomes:

$$\eta(\phi,\sigma,U_a) = (\phi_0-\phi)^{-2}\mathscr{F}\left(\frac{C(\phi)e^{-(\sigma_0^*+\sigma_a^*(U_a))/\sigma}}{\phi_0-\phi}\right). \qquad (4)$$

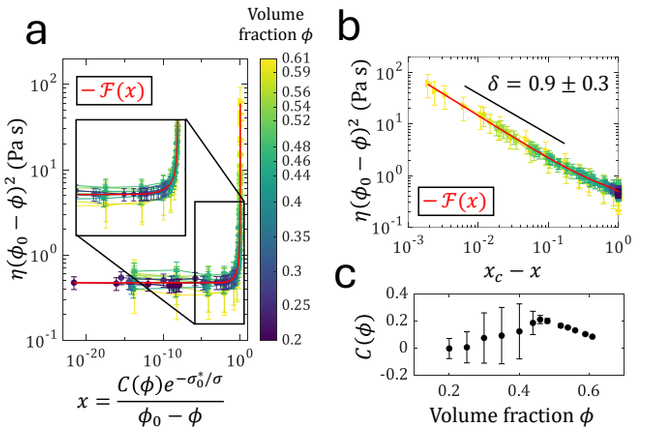

FIG. 2. Shear thickening is a precursor to shear jamming and is controlled by a crossover scaling function. (a) Viscosity data in the absence of an acoustic field ($U_a=0$) plotted as $\eta(\phi_0-\phi)^2$ versus $x=\frac{C(\phi)e^{-\sigma_0^*/\sigma}}{\phi_0-\phi}$. As predicted by Equation 2, the data collapse onto a single curve, $\mathscr{F}(x)$, whose shape is approximated by a fitting function shown as a red line (the functional form is described in the Supplementary Material, see Equations S8 and S9). The inset shows the part of the scaling function near $x=x_c=1$, where the scaling function diverges. (b) $\eta(\phi_0-\phi)^2$ versus x_c-x, highlighting that $\mathscr{F}(x)$ diverges at x_c as $\mathscr{F}\sim(x_c-x)^{-\delta}$ where $\delta=0.9\pm0.3$. (c) $C(\phi)$, the anisotropy factor plotted against volume fraction ϕ.

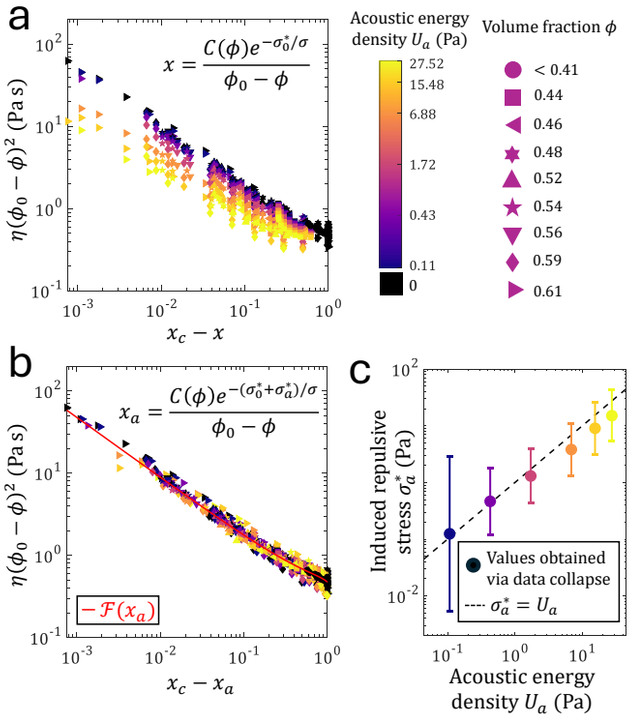

FIG. 3. The effect of acoustic perturbations may be incorporated into a universal scaling framework. (a) $\eta(\phi_0-\phi)^2$ plotted against x_c-x before incorporating the effects of acoustic perturbations. Acoustic energy density U_a is shown by the color bar. Volume fraction is shown by symbols (same symbols as Fig. 1b). The viscosity data do not collapse onto a single curve. Error bars are excluded for visual clarity. (b) After incorporating the effects of acoustic perturbations into the scaling variable x_a, the data now collapse onto the curve $\mathscr{F}(x_a)$. The red line approximates the shape of the scaling function (the functional form is described in the Supplementary Material, see Equations S8 and S9). (c) The acoustic contribution σ_a^* to the interparticle repulsive stress versus acoustic energy density U_a. The circles are the values that produce the best collapse of the viscosity data, and the dotted line is $\sigma_a^*=U_a$.

As before, we use a least-squares fitting procedure to determine the values of the parameters ϕ_0, $C(\phi)$, σ_0^*, and $\sigma_a^*(U_a)$. This approach produces an excellent collapse of the data across all volume fractions, shear stresses, and strengths of acoustic perturbations, as shown in Fig. 3b. The successful collapse is consistent with the hypothesis that acoustic perturbations provide an additional effective repulsion between particles that must be overcome by the shear stress to facilitate frictional interactions that generate thickening.

Finally, we find that the acoustic contribution to the interparticle repulsive stress $\sigma_a^*(U_a)$ is approximately equal to the acoustic energy density, that is, $\sigma_a^*\sim U_a$ (see Fig. 3c). This relation, which can be argued from dimensional analysis, is to be expected for any interparticle interaction driven by acoustics. Collectively, these results indicate that acoustic perturbations can be easily folded into the universal framework organizing thickening transitions.

This scaling framework provides a complete theory for how changes in the viscosity arise from the combined contributions of volume fraction, shear stress, and acoustic perturbations. As such it can be used practically to predict the effect of acoustic perturbations on the viscosity of a shear thickening suspension. We explicitly generate these predictions from Equation 4. This calculation requires a functional form for the scaling function $\mathscr{F}(x)$. We infer this functional form by fitting to the shape of the collapsed data (the fitting procedure is described in the Supplementary Material). The resultant function is shown as a red line in Fig. 3b. Using this functional form, along with the parameters discovered in the data collapse procedure, we observe excellent agreement between the predictions of Equation 4 and the experimental dataset, as can be seen in Fig. 4.

IV. DISCUSSION

We find that the effect of acoustic perturbations can be incorporated into a universal scaling framework for shear thickening by simply modifying σ^* to account for an additional effective interparticle repulsive barrier. Therefore we propose that suspensions dethicken under acoustic perturbation because the acoustic field induces a stronger interparticle repulsion, causing some particles to switch from frictional contact to a lubricated interaction, thereby facilitating flow and lowering the viscosity. Furthermore, we find that the additional repulsive stress σ_a^* induced by the acoustic perturbation is nearly equal to the average acoustic energy density U_a.

It is interesting to speculate about possible underlying

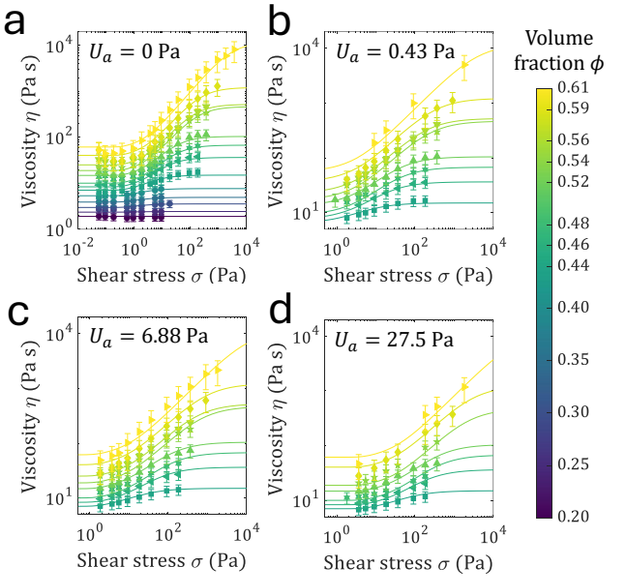

FIG. 4. Comparison between experimental measurements (symbols) and predictions of the scaling framework (lines) for suspension viscosity η as a function of volume fraction ϕ, shear stress σ, plotted for various values of the acoustic energy density U_a : (a) $U_a = 0$, (b) $U_a = 0.43\,\text{Pa}$, (c) $U_a = 6.88\,\text{Pa}$, and (d) $U_a = 27.5\,\text{Pa}$. Results for other acoustic energy densities can be found in the Supplementary Material.

mechanisms that provide this effective interparticle repulsion. First, we note the similarity of our result to an earlier study by Garat et al. which found that lower-frequency (10-50 Hz) vibrations can unjam dense suspensions by supplying an effective interparticle repulsive stress[28]. Garat et al. attributed this repulsion to effective Brownian-like forces arising from diffusive motion, which has been observed in vibrated dry granular media[29,31]. This Brownian-like repulsion scales with the kinetic energy injected by vibrations, which is consistent with our finding that the acoustically-induced repulsion scales with the acoustic energy density. If the effective repulsion we observe can also be attributed to diffusive motion of the particles, it would unify under a single mechanism the unjamming and dethickening effect of mechanical vibrations across five orders of magnitude in frequency.

At the ultrasound frequencies we study, other possible physical mechanisms may also contribute to this effective repulsion. One possibility is microstreaming, the creation of vortical flows near the particle surface, which is known to give rise to pairwise interparticle forces[54]. The magnitude of these forces is on the order of $F \sim U_a R^2$, with R being the particle radius[54]. The corresponding stress over the surface of a particle is on the order of $\sigma \sim F/R^2 \sim U_a$. Thus the interparticle stresses arising from microstreaming are expected to scale with U_a, consistent with our data. Microstreaming interactions may be attractive or repulsive depending on the Stokes number $\Omega = (2\pi f)R^2\rho_s/\eta_s$ where ρ_s and η_s are the density and viscosity of the solvent. For our system, which includes a range of particle sizes, Ω ranges from roughly 0.01 to 2. Over this range of Ω, microstreaming is expected to induce attraction in the axial direction, repulsion in the transverse direction, and a torque which tends to rotate pairs of particles towards the transverse direction. Therefore, one can imagine that the acoustically-induced two-particle torque causes an excess of particle pairs oriented in the transverse direction, where they experience a repulsive interaction. Of course, in dense suspensions, multi-particle interactions will likely complicate this picture. However, complex microscopic interactions often give rise to surprisingly simple emergent behavior in dense suspensions.

The scaling model we present describes the effect of an acoustic field on our suspensions' viscosity as a simple modification to the numerator of the scaling variable, which has been interpreted as one of the relevant renormalization group flow directions. The suspension viscosity is therefore described by the same scaling function $\mathscr{F}$ before and after the perturbation, and the acoustic field shifts the location of the shear jamming transition, but otherwise does not alter the critical behavior. We note, however, that this theory is specific to the suspension's steady state response to the acoustic field under constant shear stress. Under more complex rheological protocols, acoustically perturbed suspensions exhibit rich dynamic and history-dependent behavior, particularly in the dense regime. For example, in shear jamming suspensions, the application of acoustic perturbations in the flowing state leads to microstructural changes that are "locked in" after the acoustic field is removed and the system jams[20]. Future research could seek to describe such behavior by drawing on the theory of dynamic critical phenomena[57,58] as well as the vast literature on memory formation in granular systems[59].

Finally, we have shown that our scaling framework has practical value as a model for the effect of acoustic perturbations; we have demonstrated this explicitly by generating predictions for the suspension viscosity at different acoustic energy densities. Because this framework is based on a universal scaling function $\mathscr{F}$, it is likely that this framework could be used for a broad class of shear thickening suspensions under acoustic perturbation. One would simply require a few initial measurements of $\eta(\phi, \sigma, U_a)$ to characterize particular system-specific details: the analysis in Section III must be followed to obtain the non-universal quantities ϕ_0, $C(\phi)$, σ_0^*, and $\sigma_a^*(U_a)$. Then, Equation 4 provides a complete description of the rheology with or without acoustics. Thus, our analysis serves as a blueprint for characterizing the effect of acoustic perturbations on any dense suspension, resulting in a quantitative model which can be used to calculate the acoustic energy density required to accomplish a given target viscosity. This capability is an important step on the path to fluid metamaterials with tunable viscosities.

SUPPLEMENTARY MATERIAL

The Supplementary Material contains additional information about the experiments and analysis, including the size distribution of the microspheres, the main sources of statistical error, additional characterization of the acoustic field, and

a description of the least-squares fitting procedure used to produce the data collapses in Fig. 2 and Fig. 3. We have also included the complete viscosity dataset used in our analysis, and a comparison with the predictions of the scaling framework for data points not shown in Fig. 4. Furthermore, the Supplementary Material includes some derivations pertaining to the critical scaling of the viscosity and the underlying renormalization group flow equations. There is also a discussion on the universality of the viscosity scaling function.

ACKNOWLEDGMENTS

We thank Christopher Ness, Jason Z. Kim, Melody X. Lim, and Shreyas Sudhaman for valuable discussions. We also acknowledge Anton Paar for use of the MCR 702 rheometer through their VIP academic research program. This material is based upon work supported by the National Science Foundation Graduate Research Fellowship under Grant No. DGE-2139899. A.R.B., N.S., S.J.T., P.K., E.Y.X.O., M.R., I.C., and J.P.S. were supported by NSF DMR-2327094.

AUTHOR DECLARATIONS

The authors have no conflicts of interest to disclose.

DATA AVAILABILITY STATEMENT

The data that support the findings in this study are available from the corresponding author upon reasonable request.

[1]E. Brown, N. A. Forman, C. S. Orellana, H. Zhang, B. W. Maynor, D. E. Betts, J. M. DeSimone, and H. M. Jaeger, "Generality of shear thickening in dense suspensions," Nature Materials **9** (2010).
[2]E. Brown and H. M. Jaeger, "Shear thickening in concentrated suspensions: phenomenology, mechanisms and relations to jamming," Reports on Progress in Physics **77** (2014).
[3]N. J. Wagner and J. F. Brady, "Shear thickening in colloidal dispersions," Physics Today **62**, 27–32 (2009), https://pubs.aip.org/physicstoday/article-pdf/62/10/27/16655247/27_1_online.pdf.
[4]N. Y. C. Lin, B. M. Guy, M. Hermes, C. Ness, J. Sun, W. C. K. Poon, and I. Cohen, "Hydrodynamic and contact contributions to continuous shear thickening in colloidal suspensions," Phys. Rev. Lett. **115**, 228304 (2015).
[5]J. R. Royer, D. L. Blair, and S. D. Hudson, "Rheological signature of frictional interactions in shear thickening suspensions," Phys. Rev. Lett. **116**, 188301 (2016).
[6]M. Wyart and M. Cates, "Discontinuous shear thickening without inertia in dense non-brownian suspensions," Phys. Rev. Lett. **112** (2014).
[7]R. Seto, R. Mari, J. F. Morris, and M. M. Denn, "Discontinuous shear thickening of frictional hard-sphere suspensions," Phys. Rev. Lett. **111**, 218301 (2013).
[8]R. Mari, R. Seto, J. F. Morris, and M. M. Denn, "Shear thickening, frictionless and frictional rheologies in non-brownian suspensions," Journal of Rheology **58**, 1693–1724 (2014), https://pubs.aip.org/sor/jor/article-pdf/58/6/1693/15612580/1693_1_online.pdf.
[9]M. Zarei and J. Aalaie, "Application of shear thickening fluids in material development," Journal of Materials Research and Technology **9**, 10411–10433 (2020).
[10]S. Gürgen, M. C. Kuşhan, and W. Li, "Shear thickening fluids in protective applications: A review," Progress in Polymer Science **75**, 48–72 (2017), topical Volume on Polymer Physics.
[11]M. Wei, K. Lin, and L. Sun, "Shear thickening fluids and their applications," Materials & Design **216**, 110570 (2022).
[12]H. Barnes, "Shear-thickening ('dilatancy') in suspensions of nonaggregating solid particles dispersed in newtonian liquids," Journal of Rheology **33** (1989).
[13]A. Yahia, "Effect of solid concentration and shear rate on shear-thickening response of high-performance cement suspensions," Construction and Building Materials **53**, 517–521 (2014).
[14]F. Toussaint, C. Roy, and P.-H. Jézéquel, "Reducing shear thickening of cement-based suspensions," Rheologica Acta **48**, 883–895 (2009).
[15]G. Bossis, P. Boustingorry, Y. Grasselli, A. Meunier, R. Morini, A. Zubarev, and O. Volkova, "Discontinuous shear thickening in the presence of polymers adsorbed on the surface of calcium carbonate particles," Rheologica Acta **56**, 415–430 (2017).
[16]P. Bourrianne, V. Niggel, G. Polly, T. Divoux, and G. H. McKinley, "Tuning the shear thickening of suspensions through surface roughness and physico-chemical interactions," Phys. Rev. Res. **4**, 033062 (2022).
[17]N. M. James, E. Han, R. A. L. de la Cruz, J. Jureller, and H. M. Jaeger, "Interparticle hydrogen bonding can elicit shear jamming in dense suspensions," Nature Materials **17** (2018).
[18]N. M. James, C.-P. Hsu, N. D. Spencer, H. M. Jaeger, and L. Isa, "Tuning interparticle hydrogen bonding in shear-jamming suspensions: Kinetic effects and consequences for tribology and rheology," The Journal of Physical Chemistry Letters **10**, 1663–1668 (2019), pMID: 30896954, https://doi.org/10.1021/acs.jpclett.9b00135.
[19]P. Sehgal, M. Ramaswamy, I. Cohen, and B. Kirby, "Using acoustic perturbations to dynamically tune shear thickening in colloidal suspensions," Phys. Rev. Lett. **123** (2019).
[20]E. Y. X. Ong, A. R. Barth, N. Singh, M. Ramaswamy, A. Shetty, B. Chakraborty, J. P. Sethna, and I. Cohen, "Jamming memory into acoustically trained dense suspensions under shear," Phys. Rev. X **14** (2024).
[21]J. R. Morillas and J. de Vicente, "Magnetorheology: a review," Soft Matter **16**, 9614–9642 (2020).
[22]N. Y. Lin, C. Ness, M. E. Cates, J. Sun, and I. Cohen, "Tunable shear thickening in suspensions," Proceedings of the National Academy of Sciences **113**, 10774–10778 (2016), https://www.pnas.org/doi/pdf/10.1073/pnas.1608348113.
[23]M. Ramaswamy, I. Griniasty, J. P. Sethna, B. Chakraborty, and I. Cohen, "Universal scaling framework for controlling phase behavior in thickening and jamming suspensions," Phys. Rev. Lett. **134**, 058203 (2025).
[24]C. Hanotin, S. Kiesgen de Richter, P. Marchal, L. J. Michot, and C. Baravian, "Vibration-induced liquefaction of granular suspensions," Phys. Rev. Lett. **108**, 198301 (2012).
[25]C. Hanotin, P. Marchal, L. J. Michot, C. Baravian, and S. Kiesgen de Richter, "Dynamics of vibrated granular suspensions probed by mechanical spectroscopy and diffusing wave spectroscopy measurements," Soft Matter **9**, 9352–9360 (2013).
[26]C. Hanotin, S. Kiesgen de Richter, L. J. Michot, and P. Marchal, "Viscoelasticity of vibrated granular suspensions," Journal of Rheology **59**, 253–273 (2015).
[27]N. Gaudel, S. Kiesgen de Richter, N. Louvet, M. Jenny, and S. Skali-Lami, "Bulk and local rheology in a dense and vibrated granular suspension," Phys. Rev. E **96**, 062905 (2017).
[28]C. Garat, S. Kiesgen de Richter, P. Lidon, A. Colin, and G. Ovarlez, "Using good vibrations: Melting and controlled shear jamming of dense granular suspensions," Journal of Rheology **66**, 237–256 (2022), https://pubs.aip.org/sor/jor/article-pdf/66/2/237/16614630/237_1_online.pdf.
[29]P. Marchal, N. Smirani, and L. Choplin, "Rheology of dense-phase vibrated powders and molecular analogies," Journal of Rheology **53**, 1–29 (2009).
[30]P. Marchal, C. Hanotin, L. J. Michot, and S. K. de Richter, "Two-state model to describe the rheological behavior of vibrated granular matter," Phys. Rev. E **88**, 012207 (2013).
[31]G. D'Anna, P. Mayor, A. Barrat, V. Loreto, and F. Nori, "Observing brownian motion in vibration-fluidized granular matter," Nature **424**, 909–912 (2003).
[32]S. Kiesgen de Richter, C. Hanotin, P. Marchal, S. Leclerc, F. Demeurie, and N. Louvet, "Vibration-induced compaction of granular suspensions," The European Physical Journal E **38**, 74 (2015).

[33]R. E. Challis, M. J. W. Povey, M. L. Mather, and A. K. Holmes, "Ultrasound techniques for characterizing colloidal dispersions," Reports on Progress in Physics **68**, 1541 (2005).

[34]V. F. Humphrey, "Ultrasound and matter—physical interactions," Progress in Biophysics and Molecular Biology **93**, 195–211 (2007), effects of ultrasound and infrasound relevant to human health.

[35]S. Kentish and M. Ashokkumar, "The physical and chemical effects of ultrasound," in *Ultrasound Technologies for Food and Bioprocessing*, edited by H. Feng, G. Barbosa-Canovas, and J. Weiss (Springer New York, New York, NY, 2011) pp. 1–12.

[36]M. Ramaswamy, I. Griniasty, D. B. Liarte, A. Shetty, E. Katifori, E. Del Gado, J. P. Sethna, B. Chakraborty, and I. Cohen, "Universal scaling of shear thickening transitions," Journal of Rheology **67**, 1189–1197 (2023).

[37]It remains an open question what factors might divide shear thickening suspensions into different universality classes. For example, one might expect rod-like particles to fall into a different universality class, as rod-like particles can become entangled and therefore their jamming behavior is qualitatively different from that of spherical particles. Indeed, shear thickening suspensions of carbon nanotubes[53] are described by a viscosity scaling function which appears to be different from the scaling function that describes silica microspheres and cornstarch[36], exhibiting a much sharper transition in the vicinity of $x = x_c$. This suggests that shear thickening of carbon nanotubes may be governed by a different universality class.

[38]J. M. Simmons, "A servo-controlled rheometer for measurement of the dynamic modulus of viscoelastic liquids," Journal of Scientific Instruments **43**, 887 (1966).

[39]J. Mewis and G. Schoukens, "Mechanical spectroscopy of colloidal dispersions," Faraday Discuss. Chem. Soc. **65**, 58–64 (1978).

[40]J. Zeegers, D. van den Ende, C. Blom, E. G. Altena, G. J. Beukema, and J. Mellema, "A sensitive dynamic viscometer for measuring the complex shear modulus in a steady shear flow using the method of orthogonal superposition," Rheologica Acta **34**, 606–621 (1995).

[41]J. Vermant, P. Moldenaers, J. Mewis, M. Ellis, and R. Garritano, "Orthogonal superposition measurements using a rheometer equipped with a force rebalanced transducer," Review of Scientific Instruments **68**, 4090–4096 (1997).

[42]L. M. Walker, J. Vermant, P. Moldenaers, and J. Mewis, "Orthogonal and parallel superposition measurements on lyotropic liquid crystalline polymers," Rheologica Acta **39**, 26–37 (2000).

[43]G. Colombo, S. Kim, T. Schweizer, B. Schroyen, C. Clasen, J. Mewis, and J. Vermant, "Superposition rheology and anisotropy in rheological properties of sheared colloidal gels," Journal of Rheology **61**, 1035–1048 (2017).

[44]S. H. Sung, S. Kim, J. Hendricks, C. Clasen, and K. H. Ahn, "Orthogonal superposition rheometry of colloidal gels: time-shear rate superposition," Soft Matter **14**, 8651–8659 (2018).

[45]E. Moghimi, J. Vermant, and G. Petekidis, "Orthogonal superposition rheometry of model colloidal glasses with short-ranged attractions," Journal of Rheology **63**, 533–546 (2019).

[46]S. Kim, J. Mewis, C. Clasen, and J. Vermant, "Superposition rheometry of a wormlike micellar fluid," Rheologica Acta **52**, 727–740 (2013).

[47]A. R. Jacob, A. S. Poulos, A. N. Semenov, J. Vermant, and G. Petekidis, "Flow dynamics of concentrated starlike micelles: A superposition rheometry investigation into relaxation mechanisms," Journal of Rheology **63**, 641–653 (2019).

[48]F. A. A. Fergusson, E. W. Guptill, and A. D. MacDonald, "Velocity of sound in glycerol," The Journal of the Acoustical Society of America **26**, 67–69 (1954).

[49]To determine whether steady state had been attained, we fit the viscosity versus time during the period the acoustic field was applied to a linear function. We took the change $\Delta\eta_{\text{transient}}$ in this linear fit over the application period, and compared to the difference $\Delta\eta_{\text{acous}}$ between the viscosity with and without the acoustic field. Trials were excluded if $\Delta\eta_{\text{transient}}/\Delta\eta_{\text{acous}}$ exceeded 20%, indicating that the transient response could not be decoupled from the steady state response.

[50]B. Widom, "Equation of state in the neighborhood of the critical point," The Journal of Chemical Physics **43**, 3898–3905 (1965), https://pubs.aip.org/aip/jcp/article-pdf/43/11/3898/18841919/3898_1_online.pdf.

[51]Intriguingly, the scaling variable $x = e^{-\sigma_0^*/\sigma}/(\phi_0 - \phi)$ is precisely what would arise from stress σ being a marginally relevant variable in the renormalization group flow about the frictionless jamming point at $(\phi = \phi_0, \sigma = 0)$ (a derivation of this result can be found in the Supplementary Material). How, then, can we interpret $C(\phi)$ as it appears in Equation 2? $C(\phi)$ may be interpreted as an analytic correction to scaling that arises due to higher order terms in the renormalization group flow of σ. Indeed, our scaling variable may be rewritten in a form where analytic corrections are incorporated directly into a transformation of the stress, $x = e^{-\sigma_0^*/\Sigma(\phi,\sigma)}/(\phi_0 - \phi)$. Here, the transformed stress is $\Sigma(\phi,\sigma) = \sigma \times \sigma_0^*/(\sigma_0^* - \sigma \ln C(\phi))$.

[52]See the Supplementary Material for a derivation relating the exponent that controls the divergence of the viscosity scaling function to the exponent that controls the divergence of viscosity with respect to volume fraction.

[53]S. C. K., S. Majumdar, and A. K. Sood, "Shear jamming and fragility in fractal suspensions under confinement," Soft Matter **18**, 8813–8819 (2022).

[54]D. Fabre, J. Jalal, J. S. Leontini, and R. Manasseh, "Acoustic streaming and the induced forces between two spheres," Journal of Fluid Mechanics **810**, 378–391 (2017).

[55]B. Wu, B. VanSaders, M. X. Lim, and H. M. Jaeger, "Hydrodynamic coupling melts acoustically levitated crystalline rafts," Proceedings of the National Academy of Sciences **120**, e2301625120 (2023), https://www.pnas.org/doi/pdf/10.1073/pnas.2301625120.

[56]N. Gaudel, S. Kiesgen de Richter, N. Louvet, M. Jenny, and S. Skali-Lami, "Bulk and local rheology in a dense and vibrated granular suspension," Phys. Rev. E **96**, 062905 (2017).

[57]B. I. Halperin and P. C. Hohenberg, "Scaling laws for dynamic critical phenomena," Phys. Rev. **177**, 952–971 (1969).

[58]P. C. Hohenberg and B. I. Halperin, "Theory of dynamic critical phenomena," Rev. Mod. Phys. **49**, 435–479 (1977).

[59]N. C. Keim, J. D. Paulsen, Z. Zeravcic, S. Sastry, and S. R. Nagel, "Memory formation in matter," Rev. Mod. Phys. **91**, 035002 (2019).